Tellus (1986), *38A*, 76–87

Entrainment due to turbulent shear flow at the interface of a stably stratified fluid

By SIAVASH NARIMOUSA[1], ROBERT R. LONG and SERGEI A. KITAIGORODSKII, *Department of Earth and Planetary Sciences, The Johns Hopkins University, Baltimore, Maryland 21218, USA*

(Manuscript received December 10, 1984; in final form May 23, 1985)

ABSTRACT

An investigation is made of the entrainment due to turbulent shear flow at the interface of a stably stratified fluid between an upper turbulent layer and a lower non-turbulent layer in which the flow is generated by a disc pump in a recirculating channel, first introduced by Odell and Kovasznay. It is found that, based on friction velocity u_* and on mean velocity U, the plots of the entrainment rates as functions of the corresponding Richardson numbers for two-fluid systems and for linearly stratified systems are in agreement and collapse, so that the two systems follow the same entrainment law. The entrainment rates of the present investigation agree with those of Kantha et al., and for the most part with entrainment rates of Kranenburg. The entrainment rates of Moore and Long are also in agreement with those of present study, as are the heat-stratified entrainment rates of Deardorff and Willis.

Using δb for the buoyancy jump and h for mixed-layer depth, limiting values of $\mathrm{Ri}_* = h\delta b/u_*^2 \cong 2000$ and $\mathrm{Ri}_u = h\delta b/U^2 \cong 20$ are obtained experimentally as $E_* = u_e/u_*$ and $E_u = u_e/U$ approach zero and turbulent entrainment ceases, in agreement with an argument of Kantha. Also, limiting values of $E_* \simeq 0.3$ and $E_u \simeq 0.03$, are found for small values of Ri_* based on an argument of Tennekes and Lumley. Although no simple power-law dependence of entrainment rates on Richardson number is obtained for the whole range of Ri_*, it was possible to obtain such dependence when the range $15 < \mathrm{Ri}_* < 1500$ is divided into 3 smaller subranges.

1. Introduction

Entrainment due to turbulent shear flow at the interface of a stably stratified fluid occurs in many situations in nature and engineering and so has great importance. For example, when wind blows over the ocean, the tangential stress generates a drift current in the upper layers of the ocean, and this current begins to entrain the stratified fluid immediately below it. A similar situation also occurs in the atmosphere in the layer near the ground and in estuaries, where lighter river water flows over heavier sea water. Another example is that of a gravity current flowing over a sloping bottom under a stratified fluid, or a gravity current flowing in or out of a fjord. Other situations in which shear flow entrains a stably stratified fluid are discussed by Ellison and Turner (1959) (hereafter ET).

ET ran experiments on entrainment due to a fresh-water surface jet over a layer of salt water, and to a heavier salt solution flowing over a sloping bottom beneath a layer of fresh water. Their plots of entrainment rates $E_u = u_e/U$ as functions of overall Richardson number $\mathrm{Ri}_u = h\delta b/U^2$ (where u_e and U are the entrainment and the mean velocities, $\delta b = g\delta\rho/\rho_0$ is buoyancy difference, h is the depth of the mixed layer, $\delta\rho$ is the density difference between the two layers, ρ_0 is the reference density and g is gravity) showed that E_u fell off rapidly as Ri_u increased up to their largest Ri_u of about 0.8.

Later, Lofquist (1960), whose aim was to study stresses near an interface between stratified fluids, described an experiment with a salt-water layer flowing beneath a pool of fresh water in a long, straight channel. He measured the variation of E_u

[1] Present address: Department of Mechanical Engineering, University of Southern California, Los Angeles, California 90089, USA.

with respect to Ri_u up to a value of Ri_u of about 13, much larger than those obtained by ET.

Kato and Phillips (1969) (hereafter KP) were the first to study entrainment in a turbulent shear flow arising from the application of a tangential stress τ to the surface of a linearly stratified system (LSS). Stress was generated by a rotating flyscreen in the upper layer of a body of salt water in an annular tank. KP found that the plots of the entrainment rate $E_* = u_e/U_*$, where $u_* = (\tau/\rho)^{1/2}$ is the friction velocity, corresponded to $E_* \propto Ri_*^{-1}$ where $Ri_* = h\delta b/u_*^2$.

Kantha et al. (1977) (hereafter KPA) used the same apparatus as KP, but with two superimposed fluids of different density (2LS). KPA found entrainment rates higher than those of KP by a factor of about two for the range $30 < Ri_* < 150$. The KPA plots indicated that E_* is a function of RI_*, but, as KPA noted, no simple power-law dependence of E_* on Ri_* was obtained.

Moore and Long (1971) (hereafter ML) investigated entrainment in a 2LS in a cyclically continuous channel. They generated equal flow rates in the top and bottom layers by injecting fluid in such a way as to drive these layers in opposite directions at a mean speed U_s. At the same time, they withdrew fluid at the same rate from the top and bottom layers to maintain the initial total depth of the fluid. In this way the interface between the two fluids was kept at its initial position as salt was transferred across it. Their plots of entrainment rate yielded $E_s = u_e/U_s$ as a function of Richardson number $Ri_s = h\delta b/U_s^2$, where h is the depth of either fluid. The approximate result was $E_s \propto Ri_s^{-1}$ for the whole range of Ri_s.

Deardorff and Willis (1982) (hereafter DW) used an apparatus similar to that of KP and KPA except with the screen at the bottom of the annulus. Unlike KP and KPA they did not measure u_* directly but used, instead, an empirical formula based on their measured mean velocities to estimate u_*. Their entrainment rates, when plotted as E_* versus Ri_*, had considerable scatter, and they chose $E_* \propto Ri_u^{-1.4}\, Ri_*^{-1/2}$ as a possible empirical relationship. DW ran both LSS and 2LS experiments and these yielded similar entrainment behaviors. Kranenburg (1984) studied entrainment in a 2LS in a straight wind flume and found $E_* \propto Ri_*^{-1/2}$.

Our present purpose is to investigate the entrainment of a stably stratified fluid in turbulent shear flow in a recirculating channel similar to that of Moore and Long, using a 2LS similar to that of KPA, as well as an LSS with a superimposed initial layer of fresh water depth h_0. In the present study the turbulent shear flow is generated by a disc pump first introduced by Odell and Kovasznay (1971). The pump drives the initially fresh upper layer and the resultant turbulent shear flow begins to entrain the lower stratified stationary layer. Such an arrangement may have the advantage of being free of secondary motion (see Scranton and Lindberg (1983)), which is found by Deardorff and Yoon (1984) to be due to uneven angular momentum distribution caused by solid body rotation of the screen across the annulus. Our preliminary experiments indicated no significant tilting of the interface anywhere around the tank in any direction. The entrainment of the stratified fluid by turbulent eddies, Kelvin-Helmholtz type instabilities and wave-breaking at the interface was clearly observed in our experiments. Our instantaneous measurements of the density profile within the mixed layer revealed the presence of a quite homogeneous mixed layer (see Fig. 3). This indicates that the entrained salt water was quickly distributed within the mixed layer by turbulent eddies and that the presence of the pump in a small portion of the tank (see Fig. 1) had a minor effect on the process of salt distribution. One disadvantage of using such a pump is the difficulty in conducting experiments at very low values of Richardson numbers, $Ri_* < 50$.

Equal attention was paid to the 2LS and LSS experiments to check the differences in the KP and KPA entrainment rates mentioned above. The mean mixed-layer velocity U and the entrainment velocity u_e were measured directly, while u_* was deduced from the mean momentum-balance equation for the homogeneous, turbulent shear flow in a manner similar to that of Price (1979) (see Section 4).

In Sections 5 and 6 we compare the results of the present investigation with earlier experiments in which the shear was generated very differently. Also in these sections, the Deardorff and Willis data are replotted to enable us to compare their results with those of KPA and the present investigation. A slightly modified treatment of the data of Moore and Long is also given to allow us to suggest a better interpretation of their results. A relationship between u_* and U is obtained by a

combination of experimental measurements and theory, enabling us to find approximate values of U for the KPA experiments in which only u_* was measured directly. In this way we obtain KPA entrainment rates based on U, and these are then compared with the entrainment rates of the above-mentioned investigators. The comparisons of the present results with other results lead us to suggest maximum values of Ri_u and Ri_* corresponding to nearly zero values of E_u and E_* on the one hand, and to suggest maximum values of E_u and E_* at nearly zero values of Ri_u and Ri_* on the other.

2. The apparatus

The apparatus consists of a recirculating water channel with a straight test section and a pump section both 2 m long as shown in Fig. 1. These two sections are joined by two semi-circular annuli of mean radii 0.45 m. The width of the channel is 0.15 m in the test section and in the semi-circular annuli, while the overall width of the center of the pump section is 0.42 m and reduces gradually to 0.15 m as it meets the semi-circular annulus joints. To keep the average width of the channel constant, two diffusers of height 0.61 m equal to the channel depth are used in the pump section. The width of the diffusers changes gradually so as to create two channels of width 0.075 m as seen in Fig. 1. To aid visualization, the test section and semi-circular annuli are constructed of transparent plexiglass. The channel was filled by gravity from two 100-gallon overhead tanks containing salt and fresh water. These tanks were filled one day before running an experiment to allow air bubbles to escape and to bring the fluids to room temperature.

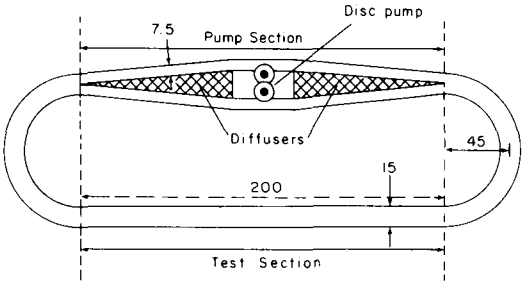

Fig. 1. Top view of the channel.

As we have mentioned, two different density stratifications were investigated. A two-layer fluid system (2LS) was produced by the same method as KPA. To produce a linearly stratified system (LSS), we first place fresh water of depth h_0 inside the channel, and then use the same method as that of ML to produce the linearly stratified layer. The result is a fresh-water layer of thickness h_0 on top of a layer of stratified fluid. The latter has a nearly linear gradient only in its upper portion (with a buoyancy frequency N averaged across the portion) but measurements of entrainment velocities were stopped at the depth at which deviation from linearity of the density profiles occurs.

The above procedure produces a LSS with zero initial density jump $\delta\rho_0 = 0$. To produce experiments with an initial $\delta\rho_o \neq 0$, the fresh-water tank was filled initially with a salt solution of density $\delta\rho_0 + \rho_0$ and the same procedure outlined above was followed.

The location of the disc pump producing the turbulent shear flow is shown in Fig. 1. For a detailed discussion of the pump manufacture and operation the reader is referred to Odell and Kovasznay (1971). The pump can generate laminar or turbulent flow by decreasing or increasing the speed of the motor. Since the purpose of this study is to generate turbulent flow, three high speeds ($F_1 < F_2 < F_3$) were used; the symbols F_1, F_2, F_3 are used only to identify the various experiments.

Fig. 2b shows the side-view of the pump section of the channel and the depth D occupied by the disc pump. The pump thickness can be varied by changing the number of discs in a given experiment. We based $D = 0.05$, 0.10 and 0.15 m. The discs drive the upper fluid only (at initial mean velocity U_0) since D is always less than the initial depth h_0. The discs are of two different diameters 0.08 and 0.26 m, but with the same thickness, 0.005 m (Fig. 2a). Because the pump's function is to drive the upper layer, a block was made so that the discs sit only on the upper part of the shafts in the initial freshwater layer. Note that the two diffusers are connected to each other by two parallel walls located immediately under the pump to allow the fluid to flow only horizontally in two channels of width 0.075 m (Fig. 1).

To visualize the mean flow, we used a thin vertical string dyed with fluorescein and then dried. The dyed string is set up in the center of the test section. As the mean flow passes the dyed line,

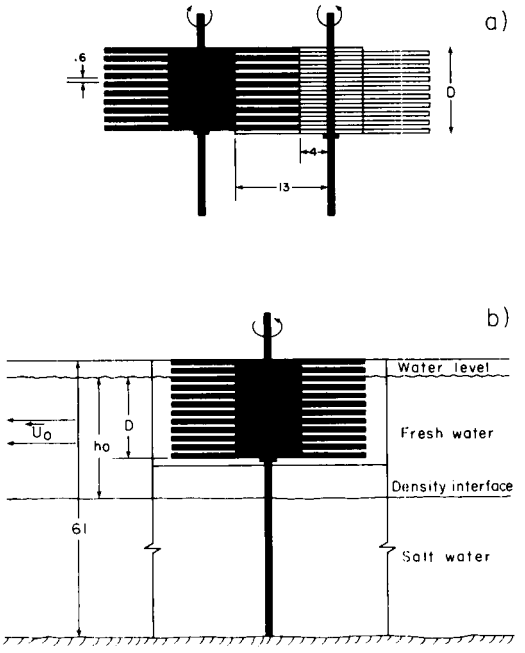

Fig. 2. (a) Downstream view of the disc pump. (b) Side view of the pump with corresponding initial conditions. Lengths in centimeters.

small amounts of dye are released. When visualization was desired, a mechanical shock on the string caused a large amount of dye to be released as a straight vertical line which immediately became irregular as it is moved horizontally by the flow. The irregular line of dye identifies the instantaneous velocity profile of the turbulent mixing layer (see Fig. 8). A light source is set up under the channel in the test section and shines through the bottom of the channel illuminating the fluorescein dye. A movie camera is used to film the illuminated dye line.

An electrical conductivity probe measures the density of the water. The tip of the probe is made of platinum wire of diameter 0.00013 m. The probe is calibrated before each experiment and was plantinized after each experiment to preserve the sensitivity of its tip. The probe was set up to travel vertically downward in the center of the channel to measure the vertical distribution of density which recorded on an x-y plotter.

The mean-flow direction is chosen as the x-direction; the vertical is along y. The conductivity probe is adjusted so that a one-centimeter vertical travel in the channel is almost exactly equal to a one-centimeter travel of the pen in the y-direction on the chart. The rate of deepening of the mixed layer was determined (Section 3) from the time-record and the recorded density profiles.

3. Measurements and observations

After a stratified system with a superimposed initial fresh-water layer is produced in the channel, the disc pump is started driving the initial fresh-water layer in turbulent shear flow. The turbulent shear flow propagates downwards behind a rapidly moving front until it meets the stratified layer at the interface between the top and the bottom layers. When the front meets a LSS having an initial zero density jump, a buoyancy jump develops and slows down the turbulent front. With the development of a stronger jump, instability similar to those of the Kelvin-Helmholtz type begins to occur at the interfacial layer, but the train of disturbances is very irregular because of the effect of the turbulence at the interfacial layer. At moderately large Richardson numbers, when the turbulence is relatively weaker, the occasional Kelvin-Helmholtz instabilities are less irregular and their presence at the interfacial layer is more evident. As the Richardson number becomes still larger, internal waves develop and finally occupy the entire interfacial layer. The disturbances are larger for higher pump speeds and smaller density jump $\delta\rho$.

The transition of the interfacial layer from pure turbulence to Kelvin-Helmholtz instabilities and finally to internal waves is accompanied by a reduction in entrainment velocity of the turbulent layer as it deepens into the stratified layer.

Fig. 3 shows recorded density profiles for a two-layer system. Figs. 4 and 5 show two typical recorded density profiles for linearly stratified systems with a zero initial density jump and with a nonzero initial density jump, respectively. These figures indicate that the turbulent layers are well mixed. The depth of the well-mixed layer h and time t in minutes are shown in the figures. The mixed-layer depth h can be determined as a function of time as shown in Figs. 6 and 7 for the 2LS and LSS experiments, respectively. The entrainment velocities, $u_e = dh/dt$, are constant for 2LS experiments but decrease as h increases in the

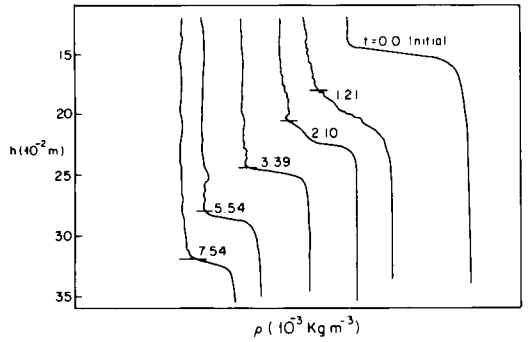

Fig. 3. Density profiles for a 2LS experiment with initial conditions $h_0 = 0.14$ m, $D = 0.15$ m, $\delta\rho_0 = 0.032 \times 10^3$ kg m^{-3} and pump speed F_3 (high) at indicated times (min). The bottom of the well-mixed layer is denoted by (–).

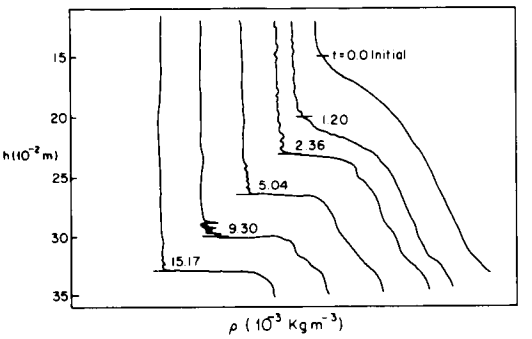

Fig. 4. Density profiles for a LSS experiment with initial conditions $h_0 = 0.14$ m, $D = 0.15$ m, $\delta\rho_0 = 0$, pump speed F_1, $N = 2.16$ between the depths 0.14 m to 0.213 m and $N = 1.77$ between the depths of 0.213 m to 0.33 m, at indicated times (min). The bottom of the well-mixed layer is denoted by (–).

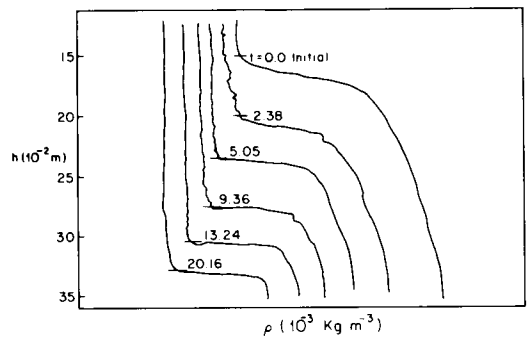

Fig. 5. Density profiles for a LSS experiment with initial conditions $h_0 = 0.15$ m, $D = 0.15$ m, $\delta\rho_0 = 0.033 \times 10^3$ kg m^{-3}, pump speed F_1 and $N = 2.15$. The bottom of the well-mixed layer is denoted by (–).

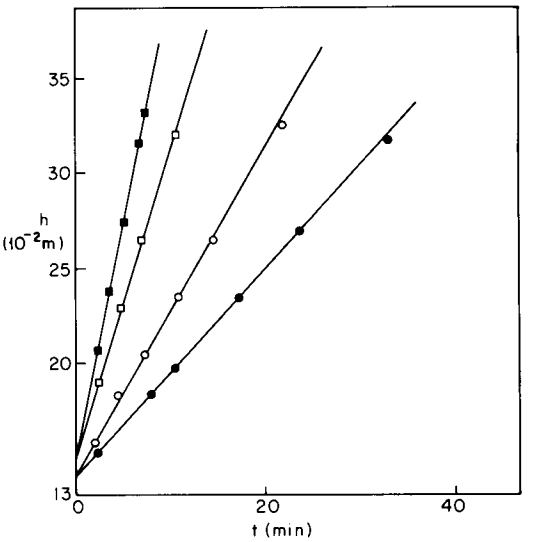

Fig. 6. Typical variations in depth h of the well-mixed layer with time for the following 2LS experiments, pump speed F_2:

	$\delta\rho_0$ (10^3 kg m^{-3})	D (m)	h_0 (m)	u_e (10^{-2} m s^{-1})
● F_2	0.091	0.15	0.14	0.0092
○ F_2	0.06	0.15	0.14	0.0145
□ F_2	0.032	0.15	0.15	0.028
■ F_2	0.022	0.15	0.15	0.043

LSS experiments. The data on Figs. 6 and 7 contain an error of about 5–10%.

In order to measure the mean, mixed-layer velocity, an area S per unit time bounded by the released dye line (photographed at a fixed time after the dyed string is shocked), the string and the free surface was measured by a Hewlett-Packard digitizer. To increase the accuracy of the direct measurements of S at a given depth, the string was shocked a number of times to reveal a number of velocity profiles (see Fig. 8). The areas of these profiles were then measured and averaged to give a single value of S at that depth. The value of U at different depths was then defined as $U \equiv S/h$. Some typical graphs of variations of S with respect to h are shown in Fig. 9 for a number of experiments. These curves have two sections. The first interval is almost linear, i.e., $\partial S/\partial h$ is constant and U slowly decreases. In the second interval, S has reached an asymptotic value and U decreases more quickly. The significance of this will be described in Section

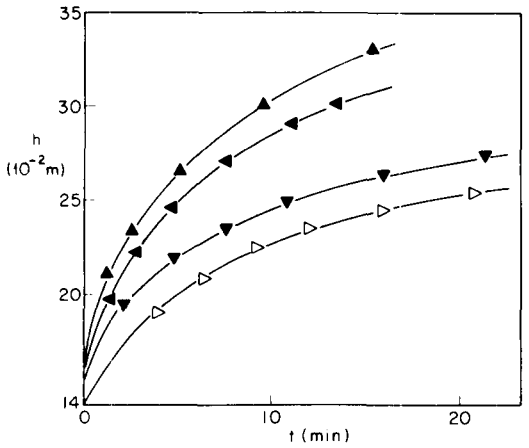

Fig. 7. Typical variations in depth h of the well-mixed layer with time for the following LSS experiments of various pump speeds.

	N (s^{-1})	D (m)	h_0 (m)	$\delta\rho_0$ (10^3 kg m^{-3})
▲ F_3	2.16	0.15	0.14	0
◀ F_3	1.82	0.10	0.145	0
▼ F_2	1.46	0.05	0.15	0
▷ F_1	1.84	0.10	0.14	0

4. Note that the data shown in Fig. 9 contain an error of about 10%.

4. The friction velocity

We consider the streamwise momentum equation for the fluid contained in the mixed layer of depth h and a thin layer below including the interfacial layer and a negligible thickness of resting fluid below. We may write

$$\frac{dS}{dt} = \frac{d(Uh)}{dt} = u_*^2 - 2w_*^2 \frac{h}{W}, \tag{1}$$

where U is the velocity defined in Section 3 and where we identify u_*, which has the dimensions of velocity, with the pressure-gradient force and the Reynolds-stress force accelerating the flow arising from the action of the pump. The second term on the right, in which W is the width of the channel, has a form introduced by Price (1979) and accounts for the retarding force of friction at the walls. We call u_* the friction velocity of the pump

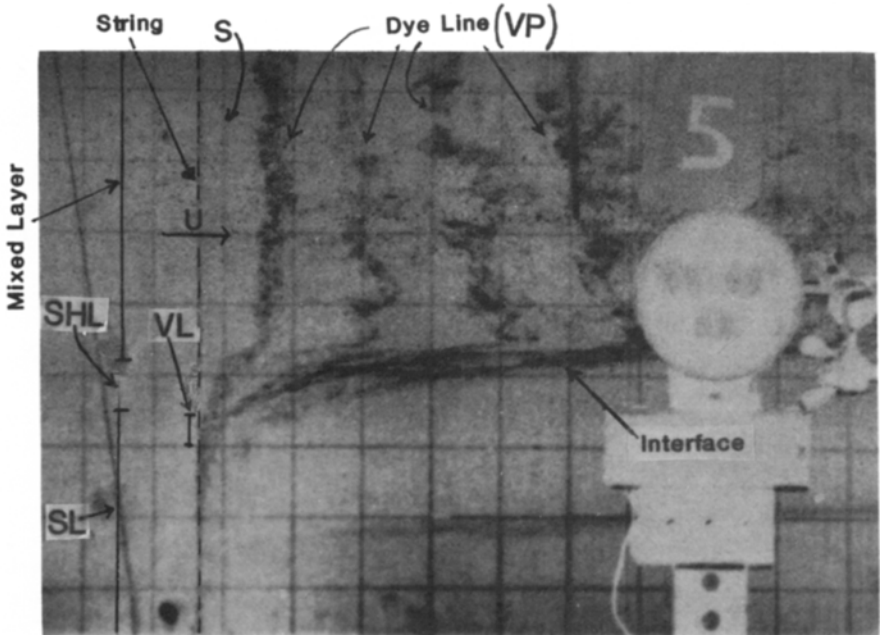

Fig. 8. Typical structure of the mean mixed-layer velocity profile (VP), with a more-or-less straight vertical section across the mixed layer and a nearly linear shear layer (SHL). The velocity approaches zero in a viscous layer (VL). In this figure (S) is the area bounded by the string, the dye line and the free surface (top of the picture), and SL stands for stationary (bottom) layer.

and w_* the friction velocity of the side walls. Using the Blasius resistance formula for turbulent channel flow (Schlichting, 1979, p. 600 and 602),

$$\frac{U}{w_*} = 8.74 \left(\frac{W}{2} \frac{w_*}{\nu} \right)^{1/7}. \tag{2}$$

Eq. (2) may be written

$$w_* = 0.15\, U^{0.875} \left(\frac{2\nu}{W} \right)^{0.125}. \tag{3}$$

Thus w_* is determined as a function of U.

The left-hand side of (1) may also be written

$$\frac{\mathrm{d}}{\mathrm{d}t}(Uh) = \frac{\partial S}{\partial h} \frac{\partial h}{\partial t}. \tag{4}$$

Since $\partial h/\partial t = u_e$ is measured, and $U_c = \partial S/\partial h$ may be obtained from Fig. 9, then, using (3), u_* may be calculated from (1). The values of u_* in any given experiment are found to increase very slowly with h as shown in Figs. 10 and 11. The differences between the lowest and highest values of u_* are in the range of 5% to 8% in a given two-layer experiment, and less than 4% in a linearly stratified experiment.

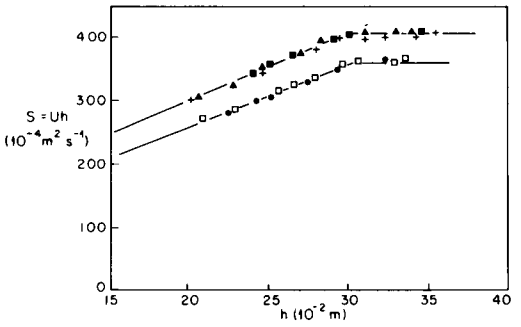

Fig. 9. Typical variations with depth h of the areas $S = Uh$ of the velocity profiles. The solid lines represent 2LS experiments with the same pump speed and D as for LSS experiments (i.e., F_2, $D = 0.15$ m for the lower curve and F_3, $D = 0.15$ m for the upper curve). The symbols for the LSS experiments are:

	N (s^{-1})	D (m)
+ F_3	1.345	0.15
▲ F_3	2.16	0.15
■ F_3	1.7	0.15
□ F_2	1.64	0.15
● F_2	1.29	0.15

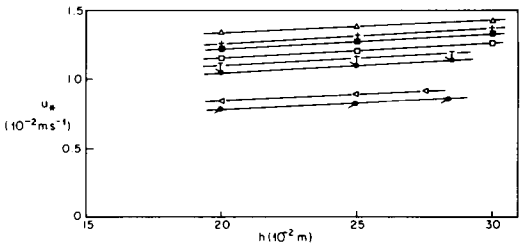

Fig. 10. Typical variation in friction velocity u_* with depth h for the 2LS experiments. The symbols represent:

	△ F_3	+ F_3	■ F_2	□ F_2	T F_3	● F_3	◁ F_3	● F_1
D(m)	0.15	0.15	0.15	0.15	0.10	0.10	0.05	0.10
$\delta\rho_0$ (10^3 kg m^{-3})	0.032	0.06	0.022	0.032	0.04	0.09	0.024	0.09

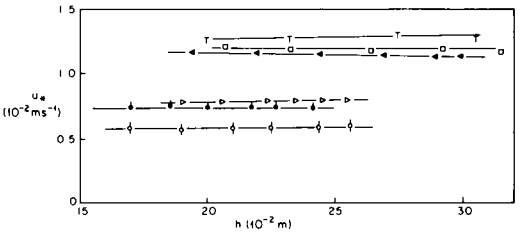

Fig. 11. Typical variations in friction velocity u_* with depth h for LSS experiments. The symbols represent:

	T F_3	□ F_2	◀ F_3	▷ F_1	● F_2	○ F_1
D (m)	0.15	0.15	0.10	0.10	0.05	0.05
N (s^{-1})	1.25	1.64	1.82	1.84	2.43	1.51

It can be seen from Fig. 10 that u_* varies considerably with variations of pump speed and D in the 2LS experiments but varies little for different choices of initial density jumps $\delta\rho_0$. This is because, at given h, the wall-term has the same value for given pump speed, D and $\delta\rho_0$, while values of $\mathrm{d}Uh/\mathrm{d}t = U_c u_e$ depend on u_e which depends on $\delta\rho_0$. In the linearly stratified experiments, for given pump speed and D, the values of u_* are insensitive to variations of buoyancy frequency N, and in Fig. 11 the plots of u_* with respect to h are shown for only one choice of N for each pair, F, D.

As we saw in Fig. 9, S is approximately constant for increasing h after a breakpoint, so that for still

larger h the left-hand side of (1) is approximately zero and (1) reduces to

$$u_*^2 = 2w_*^2 \frac{h}{W}. \tag{5}$$

In this limit the driving force of the disc pump is balanced by the wall effect. As the interest in this investigation is in the variation of h with time before u_e is influenced seriously by side-wall drag, we ignore the data after the breakpoint.

The values of u_* in all experiments were in the range.

$$10 < \frac{U}{u_*} < 11.28. \tag{6}$$

The range in (6) is not large and we use, as an average,

$$U \simeq 10.65\, u_*. \tag{7}$$

5. Entrainment results based on u_*

In the KP or KPA experiments, u_*^2 in (1) is the stress caused by the rotating screen at the surface and is held constant during the course of a given experiment. Since u_*^2 is associated with the Reynolds stress, $-\overline{u'w'}$, and since u' and w' are probably of similar magnitudes in the (nearly) homogeneous mixed layer, u_* is proportional to the turbulent velocities of the eddies σ_u. The entrainment velocity should be a function of this velocity $\sigma_u \sim u_*$ and of the eddy size l, which should be proportional to the mixed layer depth h, and of the buoyancy jump δb across the interface. Thus

$$\frac{u_e}{u_*} = f(\mathrm{Ri}_*), \qquad \mathrm{Ri}_* = \frac{h\delta b}{u_*^2}. \tag{8}$$

This is supported by the results of the KP and KPA experiments. In the present experiment u_*^2 has a different character but plays an analogous role and is, moreover, nearly constant during the course of an experiment. If the flow were non-turbulent and friction negligible, the horizontal pressure-gradient force and the gradient of $u'w'$ would be zero and u_*^2 would be zero. Therefore, still neglecting viscosity, the u_*^2 must be associated with the turbulence, and we conclude that $u_* \sim \sigma_u$ also in the present case. Consequently, we may accept (8) for the present experiment.

The calculation of u_* is given in Section 4 and $u_e = \partial h/\partial t$ and h itself are observed directly. The buoyancy jumps $\delta b = g\delta\rho/\rho_0$ are obtained from the mean buoyancy conservation equation. Since there is no buoyancy flux at the free surface, the conservation of mean buoyancy implies that

$$h\delta b = \frac{N^2}{2}(h^2 - h_0^2) + h_0 \delta b_0, \tag{9}$$

where $N^2 = \mathrm{d}b/\mathrm{d}z$ is the constant buoyancy gradient in the undisturbed fluid and h_0, δb_0 are the initial depth and the initial buoyancy jump. In general, since N, h_0, δb_0 are known and the mixed-layer depth h can be estimated from the recorded density profile, $h\delta b$ can be directly calculated from (9) in the LSS experiments. In the 2LS experiments, $N = 0$ in (9) and $h\delta b$ is constant throughout the experiment.

Fig. 12 shows plots of the entrainment rates u_e/u_* versus Ri_* for the present 2LS (closed circles) and LSS (dots) experiments. We see that the entrainment rates are the same for both systems in contrast with KP and KPA who found considerably lower entrainment rates for the LSS (KP) experiments, as we have mentioned in Section 1. The 2LS experiments of KPA and for the most part those of Kranenburg (1984) agree with our present

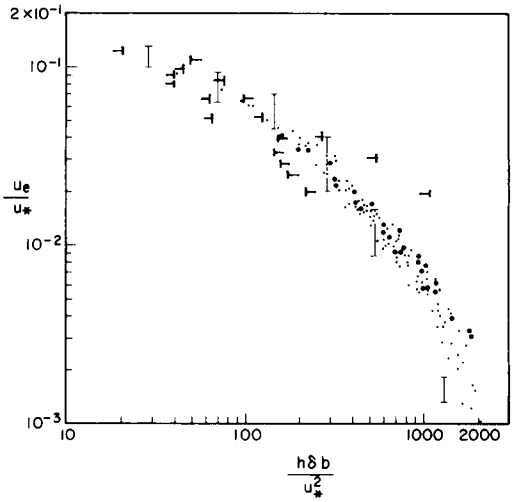

Fig. 12. The variation of entrainment rate with overall Richardson number Ri_*. The (I), (⊣) and (●) symbols represent the 2LS entrainment rates of the KPA, Kranenburg and the present study, respectively, while the (⊢) and (·) symbols represent the LSS entrainment rates of DW and the present study.

results, as do the LSS experiments of DW when u_* estimated from (1) is used to scale their measurements (see Fig. 12). DW also claim that there are similar behaviors of their 2LS and LSS experiments. We emphasize the comparison between the two types of experiments because of the considerable discussion of the problem in the literature. Thus Linden (1975) also found lower entrainment rates in the LSS case in experiments with an oscillating grid. Linden and KPA have suggested that the lower entrainment rates could be associated with energy losses in the turbulence from radiation by internal waves in the linearly stratified fluid below. Kantha (1978), Price (1979), Kitaigorodskii (1981) and Deardorff and Willis (1982) have given other explanations.

Notice that the data of Fig. 12 indicate that u_e/u_* is a function of Ri_* but that there is no simple power-law relationship. Tennekes and Lumley (1972, p. 192) suggested that $u_e/u_* \simeq 0.3$ is appropriate for entrainment in a homogeneous fluid. This provides an upper limit for entrainment in a stratified fluid. It is clear that u_e/u_* should approach the Tennekes and Lumley behavior as Ri_* approaches zero and in Fig. 12 the experimental results of KPA and the present study indicate a corresponding leveling-off of the entrainment rate as Ri_* becomes small, as one would expect.

At very high values of Ri_*, turbulent entrainment must ultimately cease and the interface advance by molecular diffusion. This provides a lower limit for entrainment. Kantha (1975) has argued that, for fully turbulent entrainment, the kinetic energy of the eddies, proportional to u_*^2, should be related to potential energy $\Delta\delta b$, needed to lift fluid elements through the interface, by

$$u_*^2 > \Delta\delta b, \tag{10}$$

where Δ is the interfacial-layer thickness (see also Phillips, 1977). At very high values of Ri_*, where the interface is flat and molecular diffusion of salt is dominant, a lower limit to Δ is k/u_e (diffusion length scale), where $k \simeq 1.2 \times 10^{-9}$ m^2 s^{-1} is the coefficient of diffusivity for salt and u_e is the speed of advance of the interface by molecular diffusion. Rearranging (10) and substituting k/u_e for Δ, we get

$$\mathrm{Ri}_* \leqslant \left(\frac{u_e}{u_*}\right)\left(\frac{u_* h}{k}\right), \tag{11}$$

where u_e/u_* is the entrainment coefficient and $\mathrm{Pe} = u_* h/k$ is the Peclet number. To estimate the maximum value of Ri_{*m}, the values $u_e/u_* \simeq 10^{-3}$ and $\mathrm{Pe} \simeq 19.3 \times 10^5$ (using $u_* = 0.008$ m s^{-1}, $h = 0.29$ m) were chosen. This yields

$$\mathrm{Ri}_{*m} \simeq 1900, \tag{12}$$

which is similar to the highest values of Ri_* in the present data at values of u_e/u_* so small that the entrainment process may well be dominated by molecular diffusion.

6. Entrainment rates based on U

We have suggested that the friction velocity u_* is the best scaling velocity, but, in a number of experiments, for example, ML, ET and Lofquist, the mean mixed-layer velocity U has been used and we should attempt to compare our present results with these using the measured U in our experiments. This presents no direct difficulty in the LSS experiments, but in the 2LS experiments we found that U decreased steadily during an experiment and, because u_e and $h\delta b$ were constants during the course of the experiment the points $(u_e/U,\ h\delta b/U^2)$ in the $E_u - \mathrm{Ri}_u$ plane moved upward and to the right. We see this in Fig. 13 in which the lower points come from the earliest times (smaller h in Fig. 9) and the upper points from the later times (just before the breakpoint in Fig. 9). Clearly if u_e/U is a function of Ri_u alone, this would not be possible, and we conclude that U must be influenced by viscosity or by the wall effect. It seems most likely from the observed behavior, which corresponds to lower U and so larger u_e/U and Ri_u at the later times, that the wall effect is primarily responsible. We may say, however, that there is general agreement between the 2LS and LSS results in the present study.

Fig. 13 contains data, based on U, from KPA and, except for KPA's lower entrainment rates at large Ri_u, there is general agreement with the present study. The U in KPA is obtained from the measured u_* by taking average values of u_e/u_* versus Ri_* in their Fig. 8 and converting to U by use of (7). Also in Fig. 3 are data of ML in which the total depth of the fluid is used to obtain comparable results. Again, these data agree well with the present study and KPA. Finally, Fig. 13 contains the LSS (heat) data of DW and for the most part

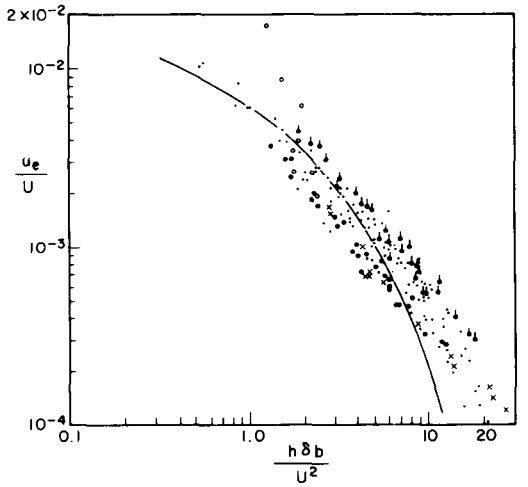

Fig. 13. Entrainment rate E_u versus Ri_u. The solid line crosses (X) represent the entrainment rates of the 2LS experiments of KPA and ML. Symbols (●) and (◐) represent the 2LS experiments of the present study based on the U calculated from the S-curves of Fig. 9 at the smallest and largest h, respectively, in the interval of linearly increasing S. The (○) and (·) symbols represent the entrainment rates of the LSS experiments of DW and the present study, respectively.

there is rough agreement with ML, KPA and the present study. The 2LS data of DW (not in Fig. 13) have considerably lower entrainment rates.

7. Power-law behavior in subranges of Ri_*

It is tempting to look for power-law behaviors in the data of entrainment but, as we have indicated, there is no such behavior over the whole range of Ri_*. We may look, however, at smaller ranges of Ri_* (see also Kantha (1975)). For example, according to Fig. 12, in the range $15 < Ri_* < 150$ of our data, we have

$$\frac{u_e}{u_*} \simeq 0.65\ Ri_*^{-1/2}, \tag{13}$$

in which the exponent agrees with the behavior $u_e/u_* \simeq 0.5\ Ri_*^{-1/2}$ suggested by Pollard et al. (1973) for the initial deepening of a mixed layer based on a closure assumption that $Ri_u = 1$. Similar theories have been advanced by Price (1979) and Mellor and Durbin (1975). Although Ri_u varies widely in all experiments, it is possible that the $-1/2$ behavior is appropriate for the lower ranges of Ri_u, in particular for our low Richardson number experiments in which (13) holds reasonably well.

For the range $150 < Ri_* < 800$, our data may be approximated by

$$\frac{u_e}{u_*} \simeq 7\ Ri_*^{-1}, \tag{14}$$

which is similar to the behavior suggested by Phillips (1977, p. 300) for the KPA data at moderate values of Ri_*; see also Cushman-Roisin (1981).

Finally, according to Fig. 12, the entrainment law for large Ri_* may be approximated by

$$\frac{u_e}{u_*} \simeq 5 Ri_*^{-3/2}. \tag{15}$$

We suggest that the three separate ranges may involve entrainment processes which are basically different. In the range of validity of (13), not only the interior of the mixed layer but also the base of the mixed layer (interface) is fully turbulent as in Fig. 14a. The mean shear is large and the density jumps are weak so that the energy-containing eddies of the mixed layer directly produce the entrainment. In the range of (14) the mixed layer is turbulent but the interface is less chaotic and, because of the greater stability, Kelvin-Helmholtz type instabilities appear as in Fig. 14b. These would tend to be less efficient than the fully turbulent eddies and so lead to a slower entrainment.

In the range of (15) (see Fig. 14c) the shear is weak and the turbulence of the mixed layer may cause an entrainment process like that of Long (1978) who considered the case of the oscillating grid (zero shear). Long found an $Ri_*^{-7/4}$ law which is close to that in (15).

Finally, in Fig. 14d the stability is very great, the interface is flat and entrainment may be by molecular processes.

8. Summary and conclusions

The importance of entrainment in atmosphere and oceans and, in particular, the importance of shear in this process has prompted a number of studies including the present one in which tur-

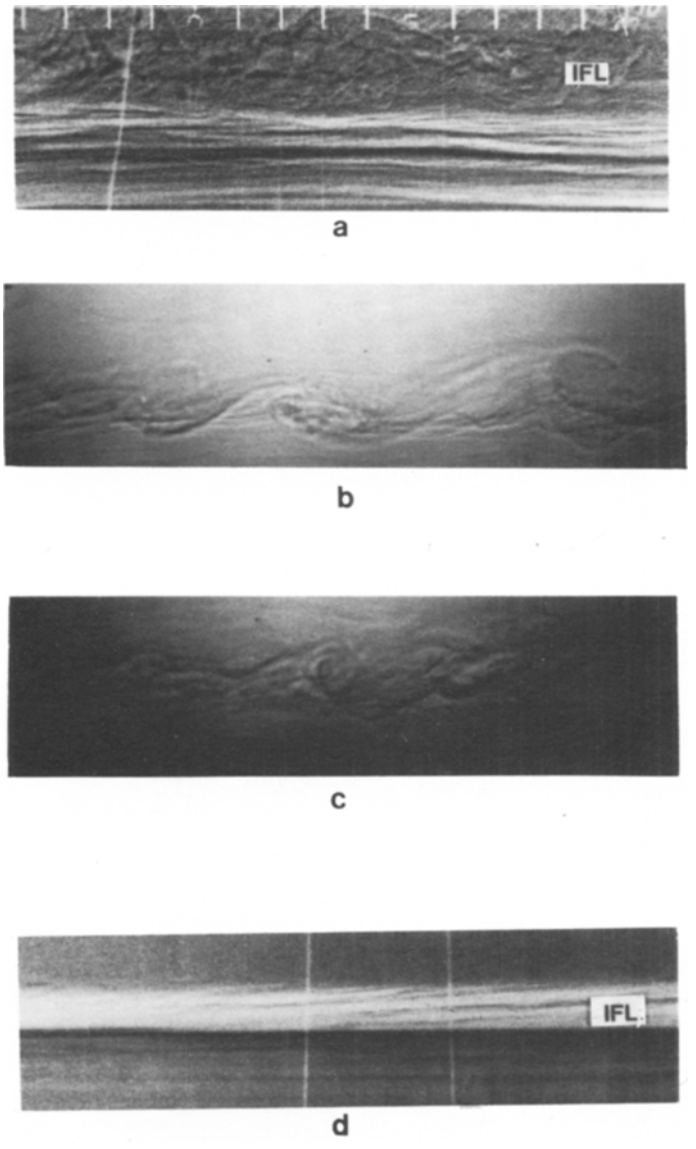

Fig. 14. (a) A fully turbulent interfacial layer at low values of Richardson number $Ri_* < 150$; (b) a turbulent interfacial layer in the presence of Kelvin-Helmholtz instabilities in the range $150 < Ri_* < 800$; (c) a breaking internal-wave-type interfacial layer in the range $800 < Ri_* < 1500$; (d) a flat interface at very high values of $Ri_* > 1500$, showing no turbulent instabilities at the interfacial layer; in this case, molecular effects may be dominant. In Figs. 14 (a–d), IFL stands for interfacial layer, and the mixed layer is in the upper portions of the photographs.

bulent flow is produced in a cyclic channel by a pump devised by Odell and Kovasznay. Measurements were made of mean velocity in the mixed layer, of salinity distributions in the vertical and of the deepening of the mixed layer. As originally suggested by Kato and Phillips (1969), the friction velocity u_*, related to the velocity of the eddies, appears to be the most fundamental velocity and we have computed an analogous quantity in our problem. We found that the entrainment velocity

scaled on u_* is a function of the corresponding Richardson number Ri_* and that the relationship is the same for both the two-layer and the linearly stratified systems of this paper. There is also agreement between the present data and that of KPA, ML, DW (LSS) and Kranenburg. The empirical relationship between u_e/u_* and Ri_* is not a simple power law but may be approximated by power laws, $Ri_*^{-1/2}$, Ri_*^{-1}, and $Ri_*^{-3/2}$ in three subranges for small, moderate and large values of Ri_*. At very small Ri_* there is a tendency for u_e/u_* to approach a constant and the behavior for very large $Ri_* \simeq 2000$ indicates a cessation of turbulent entrainment as molecular diffusion tends to dominate.

Finally we were able to compare the results of the present experiment, expressed in terms of u_e/U and $Ri_u = h\delta b/U^2$, where U is mean velocity in the mixed layer, with data from Moore and Long (1971) and from Kantha et al. (1977) and we found general agreement.

9. Acknowledgements

We are grateful to Professor O. M. Phillips for his valuable comments and support for the laboratory part of this study. The first author wishes to thank Professor T. Maxworthy for his kindness, L. Kantha for his suggestions and Sniti Onida for his laboratory assistance. Financial support was from The National Science Foundation, Grants OCE-8405306 and ATM 8210498 and from the Office of Naval Research, Fluid Dynamics Branch, N00014-76-C-0184.

REFERENCES

Cushman-Roisin, B. 1981. Deepening of the wind-mixed layer: a model of the vertical structure. *Tellus 33*, 564.

Deardorff, J. W. and Willis, G. E. 1982. Dependence of mixed-layer entrainment on shear stress and velocity jump. *J. Fluid Mech. 115*, 123–150.

Deardorff, J. W. and Yoon, S. C. 1984. On the use of an annulus to study mixed-layer entrainment. *J. Fluid Mech. 142*, 97.

Ellison, T. H. and Turner, J. S. 1959. Turbulent entrainment in stratified flows. *J. Fluid Mech. 6*, 423–448.

Kantha, L. H. 1975. Turbulent entrainment at the density interface of a two-layer stably stratified fluid system. *Earth and Planetary Sciences*, GFDL, Rep. 75–1.

Kantha, L. H. 1978. On surface-stress-induced entrainment at a buoyancy interface. *Earth and Planetary Sciences*, GFDL, Rep. 78–1.

Kantha, L. H., Phillips, O. M. and Azad, R. S. 1977. On turbulent entrainment at a stable density interface. *J. Fluid Mech. 79*, 753–768.

Kato, H. and Phillips, O. M. 1969. On the penetration of a turbulent layer into stratified fluid. *J. Fluid Mech. 37*, 643–655.

Kitaigorodskii, S. A. (1981). On the theory of the surface-stress induced entrainment at a buoyancy interface (toward interpretation of KP and KPA experiments). *Tellus 33*, 89–101.

Kranenburg, C. 1984. Wind-induced entrainment in a stably stratified fluid. *J. Fluid Mech. 145*, 253–273.

Linden, P. F. 1975. The deepening of a mixed layer in a stratified fluid. *J. Fluid Mech. 71*, 385–405.

Lofquist, K. 1960. Flow and stress near an interface between stratified fluids. *Phys. Fluids 3*, 158–175.

Long, R. R. 1978. A theory of mixing in a stably stratified fluid. *J. Fluid Mech. 84*, 113–124.

Mellor, G. L. and Durbin, P. A. 1975. The structure and dynamics of the ocean surface mixed layer. *J. Phys. Oceanogr. 5*, 718–728.

Moore, M. J. and Long, R. R. 1971. An experimental investigation of turbulent stratified shearing flow. *J. Fluid Mech. 49*, 635–655.

Odell, G. M. and Kavasznay, L. S. G. 1971. A new type of water channel with density stratification. *J. Fluid Mech. 50*, 535–543.

Phillips, O. M. 1977. *Dynamics of the upper ocean*, 2nd edition. Cambridge University Press.

Pollard, R. T., Rhines, P. B. and Thompson, R. O. R. Y. 1973. The deepening of the wind-mixed layer. *Geophys. Fluid Dyn. 3*, 381–404.

Price, J. F. 1979. On the scaling of stress-driven entrainment experiments. *J. Fluid Mech. 90*, 509–529.

Schlichting, H. 1979. *Boundary layer theory*, McGraw-Hill, New York.

Scranton, D. R. and Lindberg, W. R. 1983. An experimental study of entraining stress-driven, stratified flow in an annulus. *Phys. Fluids 26*, 1198.

Tennekes, H. and Lumley, J. L. 1972. *A first Course in turbulence*. The MIT Press.